ResearchGate

See discussions, stats, and author profiles for this publication at: https://www.researchgate.net/publication/268205476

Transport in biological systems

Article *in* Journal of the Serbian Society for Computational Mechanics · January 2011

CITATIONS
27

READS
6,324

8 authors, including:

Milos Kojic
Houston Methodist Hospital
140 PUBLICATIONS **2,367** CITATIONS

SEE PROFILE

Miljan Milosevic
University of Kragujevac
98 PUBLICATIONS **876** CITATIONS

SEE PROFILE

Velibor Isailovic
University of Kragujevac
62 PUBLICATIONS **212** CITATIONS

SEE PROFILE

Nikola Kojic
Massachusetts Institute of Technology
37 PUBLICATIONS **2,483** CITATIONS

SEE PROFILE

All content following this page was uploaded by Milos Kojic on 19 November 2014.

The user has requested enhancement of the downloaded file.

Journal of the Serbian Society for Computational Mechanics / Vol. 5 / No. 2, 2011 / pp. 101-128
(UDC: 577.3)

Transport in biological systems

M. Kojic[1,2], A. Ziemys[2], M. Milosevic[1], V. Isailovic[1], N. Kojic[4,5], M. Rosic[3], N. Filipovic[3], M. Ferrari[2]

[1]Metropolitan University, Belgrade – R & D Center for Bioengineering, 34000 Kragujevac, Serbia
[2]The Methodist Hospital Research Institute, Houston, TX 77030
[3]University of Kragujevac
[4]Tufts University, Medford, MA 02155, 5 – Metropolitan University, Belgrade

Abstract

Transport of matter in biological systems represents the vital and most important process. The transport occurs in different scales, spanning from the atomic to macroscale. It is very complex since it involves both biochemical and mechanical sources. Modeling remains a challenge due to this complexity. In this report we refer to the following specific topics: diffusion in complex media, transport of solid bodies by fluid, and transport of distributed matter by fluid. Those are the topics on which the research has been performed at The Methodist Hospital Research Institute, Houston; and at Metropolitan University, Belgrade – R & D Center for Bioengineering, Kragujevac. The methodology for diffusion relies on a hierarchical modeling approach introduced in [Ziemys et al. 2011] which accounts for interface effects between solid phase and transported molecules. Here, a generalization of the hierarchical approach is proposed for diffusion in composite media. We employ a remeshing concept to model transport of deformable bodies (biological cells, as red blood cells) or rigid bodies (nano- or micro-particles) within fluid as blood. And we employ transport equations, coupling fluid flow and diffusion, for transport of distributed matter as biological proteins within blood.

Keywords: diffusion, molecular transport, molecular dynamics, finite element method, transport of biological cells, remeshing method, transport of distributed matter

1. Transport by passive diffusion

We here present the basic concept of modeling diffusion in nanospace, following [Ziemys et al. 2011] and [Kojic et al. 2011], and then outline a generalization of this concept to composite (polymer) media.

1.1 General

In common continuum theories of diffusion through homogenous media Fick's law is used as the fundamental relation:

$$J = -D\nabla c \tag{1}$$

where $\boldsymbol{J}$ is the mass flux along concentration gradient ∇c with diffusion coefficient (diffusivity) D. The Stokes-Einstein relation shows that D for an ideal (non-interactive) solution is proportional to molecular mobility μ and thermal energy $k_B T$, or it is inversely proportional to viscosity η and radius r of the diffusing molecule. In real conditions, it is experimentally found that D depends on concentration, i.e. D=D(c) (English and Dole 1950, Alpert and Banks 1976). However, in nanoconfinement, phase interface may occupy a substantial portion of diffusion domain so that diffusion transport is affected by molecular interactions with the surface, and predictions following Eq. (1) may become inaccurate.

MD modeling and experiments have shown that diffusive transport of molecules and particles in nanochannels is affected by their proximity to a solid surface [Ziemys et al. 2010], [Aggarwal et al. 2007]. Using MD analysis, it is shown in [Ziemys et al. 2010] that molecular diffusivity depends on both concentration and confinement effects. Therefore, modeling of these transport regimes needs novel approaches that could bring molecular scale information into complex macroscale models of nanofluidic devices. MD provides insight into the physics of molecular transport, but it can be used for modeling very small regions, therefore macroscopic methods are necessary. An ideal scenario is to properly transfer MD information to macroscopic models; hierarchical (multiscale) models offer this possibility.

Among various continuum-based numerical methods, which in essence employ a discretization concept, the most developed and well established is the Finite Element Method (FEM). A time and length scale is usually several orders of magnitude larger than in MD. Various schemes have been introduced to couple MD and FEM, as hybrid methods [Rudd and Broughton 1998], [Hou and Wu 1997], [Broughton et al. 1999], or bridging scale methods [Wagner and Liu 2003], [Kojic et al. 2006a, 2008a,b].

Next, we first outline MD simulations, then the FEM, followed by bridging MD-FEM, and finally a generalization of the hierarchical model to diffusion within composite media .

1.2 MD simulations and scaling function for diffusion coefficient

Molecular Dynamics (MD) has been used for several decades [Rapaport 2004]. It is based on statistical mechanics, where motion of particles is described according to the Newtonian mechanics:

$$m_i \dot{\mathbf{v}}_i = \mathbf{F}_i \tag{2}$$

where m_i, $\dot{\mathbf{v}}_i$ and $\mathbf{F}_i$ are mass, acceleration and resulting force (including interaction forces from the neighboring particles and external forces), respectively. The interaction forces include bonded (repulsive-attractive, bending and torsional) and non-bonded (electrostatic, van der Waals) terms. The Force Field (FF) represents a functional form of behavior of chemical structures and is evaluated from potential energy function, $E = E_{intra} + E_{inter}$, of CHARMM FF (MacKerell et al. 1998) which is used in our MD models.

MD simulations for calculating diffusivities in nanochannels were carried out [Ziemys et al. 2009, 2010] using NAMD 2.6 [Phillips et al. 2005] with a TIP3P water model [Jorgensen et al. 1983] and NVT (fixed number of particles N, pressure P, volume V) ensembles. CHARMM compatible amorphous silica force field [Cruz- Chu et al. 2006] was employed to model the silica nanochannel, which is modeled by charged hydrophilic amorphous silica phase to match the silica properties after the fabrication process. Glucose diffusion coefficients were calculated from 30 ns trajectories by using the mean square displacement $<r^2>$:

$$< r^2 >= 2dDt \tag{3}$$

where the factor d = 1, 2, 3 depends on the dimensionality of the space, and t is time. The diffusivity along the surface normal (z-direction) was evaluated, from the surface up to the middle of the nanochannel. The time window t for $<r^2>$ was chosen as 20 ps, which is small enough to catch local displacements within 0.5 nm thick slabs. The diffusivity results include dependence on distance from the wall and glucose concentrations (Fig 1 – left panel).

The MD calculated diffusivity is normalized with respect to the "bulk" value D_{bulk} corresponding to diffusivity far from the surface, where influence of the surface is negligible. Hence, we have

$$D = SD_{bulk} \tag{4}$$

where

$$S = S(h, c),\ 0 \le S \le 1 \tag{5}$$

is the scaling function which depends on the distance from the wall surface h and concentration c. Calculated scaling function is shown in Fig. 1 – right panel.

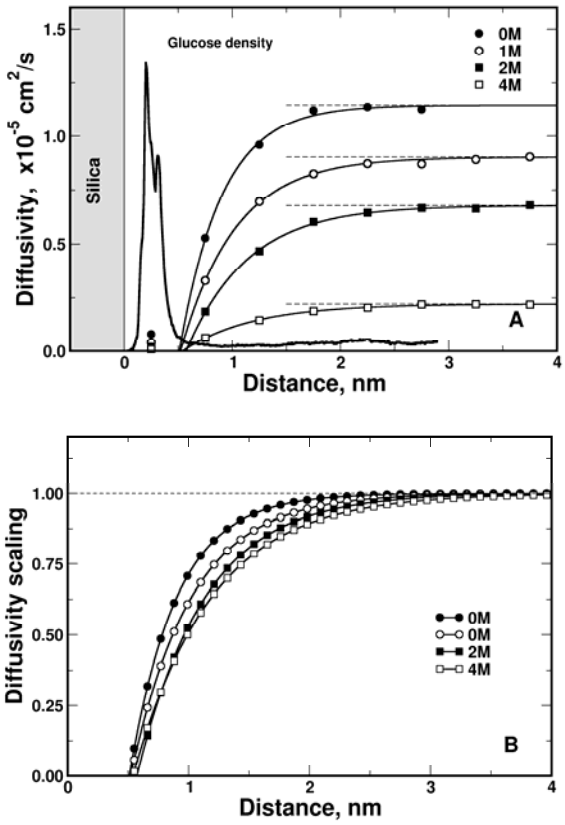

Fig. 1. Calculated glucose diffusivity (left panel)) and scaling functions of the proximity to the silica surface for several concentrations (right panel); according to Ziemys et al. (2011)

Experimental investigations showed that $D(\equiv D_{bulk})$ for glucose depends on concentration, although data are quite different (see [Ziemys et al. 2011] and references given therein). For examples shown here we have chosen the glucose D according to the largest data set of [Gladden and Dole, 1953] that spans over a wide range of concentrations, from 0 to 3.36 M, with linear dependence D(c).

1.3 Finite element model

We here consider unsteady diffusion where the diffusion coefficient depends on both concentration and spatial position of a point within the model. FE solution procedures for nonlinear diffusion problems have been well established and successfully used in various applications [e.g. Bathe 1996, Hughes 2000], [Kojic et al. 2006b, 2008a]. The basic mass balance equation, which also includes Fick's law in equation (1), is is transformed into the incremental-iterative system of linear balance equations for a finite element [Kojic et al. 2008a]:

$$\left(\frac{1}{\Delta t}\mathbf{M} + {}^{n+1}\mathbf{K}^{(i-1)}\right)\Delta\mathbf{C}^{(i)} = {}^{n+1}\mathbf{Q}^{S(i-1)} + {}^{n+1}\mathbf{Q}^{V(i)} - {}^{n+1}\mathbf{K}^{(i-1)}\,{}^{n+1}\mathbf{C}^{(i-1)} - \frac{1}{\Delta t}\mathbf{M}\left({}^{n+1}\mathbf{C}^{(i-1)} - {}^{n}\mathbf{C}\right) \tag{6}$$

where $\mathbf{C}$ is the vector of nodal concentrations; the left upper indices n and n+1 denote values at the start and end of the time step n of size Δt; the indices i and i-1 correspond to the current and previous equilibrium iteration; $\mathbf{Q}^S$ and $\mathbf{Q}^V$ are surface and volumetric nodal fluxes for the element; and components of the matrices $\mathbf{M}$ and $\mathbf{K}$ are

$$M_{IJ} = \int_V N_I N_J dV \tag{7}$$

$${}^{n+1}K_{IJ}^{(i-1)} = \int_V {}^{n+1}D^{(i-1)} N_{I,i} N_{J,i} dV \tag{8}$$

Here N_I and N_J are the interpolation functions, and ${}^{n+1}D^{(i-1)}$ is the diffusion coefficient corresponding to the last known concentration ${}^{n+1}c^{(i-1)}$ at a point within the finite element. Assembly of equations (6) and solution procedures are performed in a usual manner that is well described in the computational mechanics literature (e.g. Bathe 1996).

In our models we have incorporated concentration and interface effects, according to equation (4) into the FEM model. Implementation of the expression (4) is illustrated in Fig. 2. Note that linear interpolation between scaling curves is used.

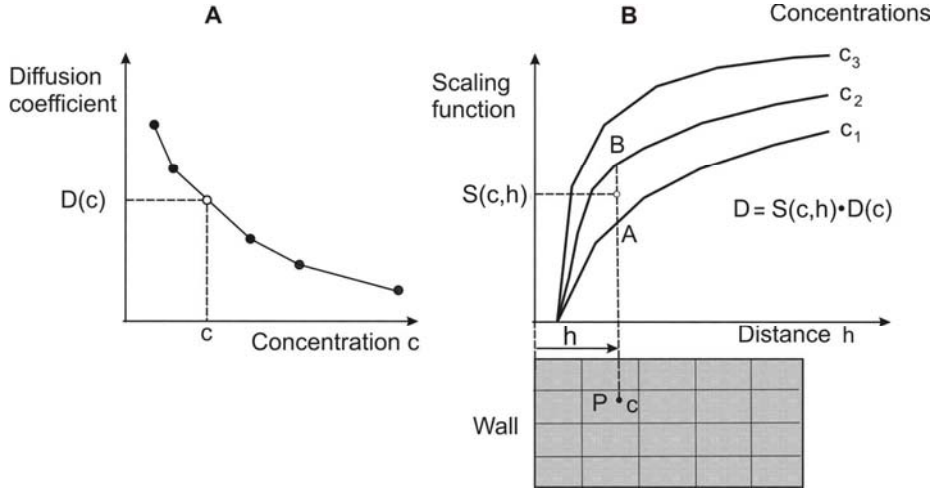

Fig. 2. Determination of diffusion coefficient at a spatial point P using dependence on concentration and surface effects. The "bulk" value is first determined from the curve $D(c)$, A; then the scaling function is evaluated form family of curves shown in B. Linear interpolation curves $S(c,w)$ is adopted (between points A and B in the figure); according to [Kojic et al., 2011].

The described hierarchical model has been verified by comparison of diffusion experiments in nanochannels [Fine et al., 2010]. Good agreement between computed and experimental results for mass release was found [Ziemys et al., 2011].

1.4 Generalization of the hierarchical model to porous media

Finally, here we outline a generalization of the hierarchical model to diffusion in complex porous media, consisting of distributed solid constituents within fluid. For simplicity of presentation of this generalization, we assume a medium with solid fibers, as sketched in Fig. 3.

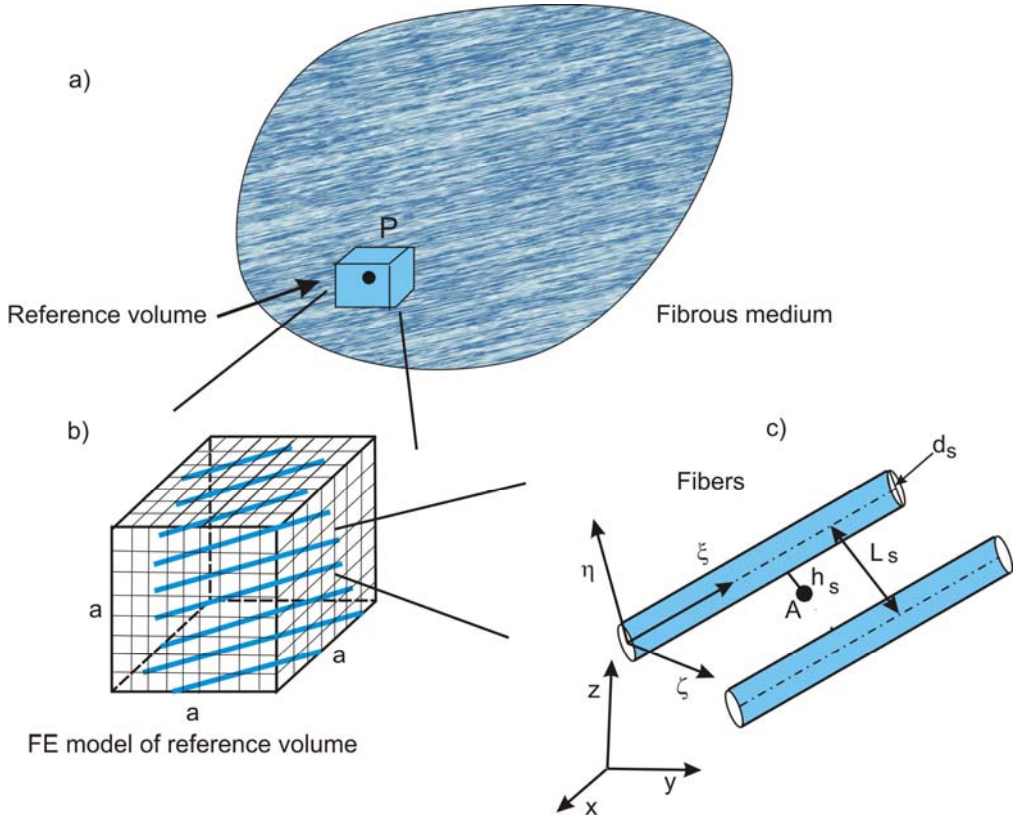

Fig. 3. Concept of extension of hierarchical model to porous medium with fibers. a) Fibrous medium with reference volume at a material point P; b) Reference volume discretized into finite elements; c) Geometry of the internal structure – fibers of a s-group, with diameter d_s and with mutual distance L_s, and point A at distance h_s from the fiber surface.

The main idea here is to determine equivalent diffusion parameters of a homogenous porous medium which capture the internal structure of a composite medium in a way that diffusion properties are preserved. To achieve this, we first take a reference volume around a material point (in a form of a cube) around that point, Fig. 3a, and discretize it into finite elements (Fig. 3b). Here we take the real internal structure and calculate diffusion in three orthogonal directions. In this FE model it is possible to properly take into account the surface effects, as sketched in Fig 3c. Namely, for a point A in the medium we calculate distance from the closest fiber surface of an s-group, and evaluate scaling function S_s as described above for diffusion within a nanochannel. We assume that scaling functions are different for the normal and tangential directions, hence we have three scaling functions S^s_ξ, S^s_η, S^s_ς in the local fiber directions ξ, η, ξ, so that the diagonal diffusion matrix (tensor) $D^s_{\xi\xi}, D^s_{\eta\eta}, D^s_{\varsigma\varsigma}$ in the local coordinate system is

$$
\begin{aligned}
D^s_{\xi\xi} &= S^s_\xi D_{bulk} \\
D^s_{\eta\eta} &= S^s_\eta D_{bulk} \\
D^s_{\varsigma\varsigma} &= S^s_\varsigma D_{bulk}
\end{aligned}
\tag{9}
$$

where D_{bulk} is the bulk modulus. The diffusion tensor in the global coordinate system *x,y,z* can be obtained by tensorial transformation of the second-order tensor,

$$\mathbf{D}^s_{xyz} = \mathbf{T}^s \mathbf{D}^s_{\xi\eta\varsigma} \mathbf{T}^{sT} \tag{10}$$

where the components of the transformation matrix contains cosines of angles between local and global axes:

$$T^s_{ij} = \cos(x_i, \xi_j)\text{, i,j=1,2,3} \tag{11}$$

Here x_i and ξ_j stand for global (*x,y.z*) and local coordinate (ξ, η, ς) systems.

Calculation of diffusion is performed assuming given concentrations on two opposite surfaces of the reference cube, with diffusion in x -, then in y -, and finally in z-direction. In these calculations we assume that entrance surface is connected to a reservoir of volume V, with initial concentration C_0^{in} ; while the opposite surface has a constant concentration $C^{out}(=0)$, Fig. 4a. The diffusion progresses until the equilibrium state is reached, with $C^{in}_{final} = C^{out}(=0)$. The mass release curves for three directions are schematically shown in Fig. 4b. This diffusion model is adopted in order to cover the whole range of concentration – from C_0^{in} to zero, and mass release rate (or fluxes through the opposite surfaces), starting from initial high values to final zero-values.

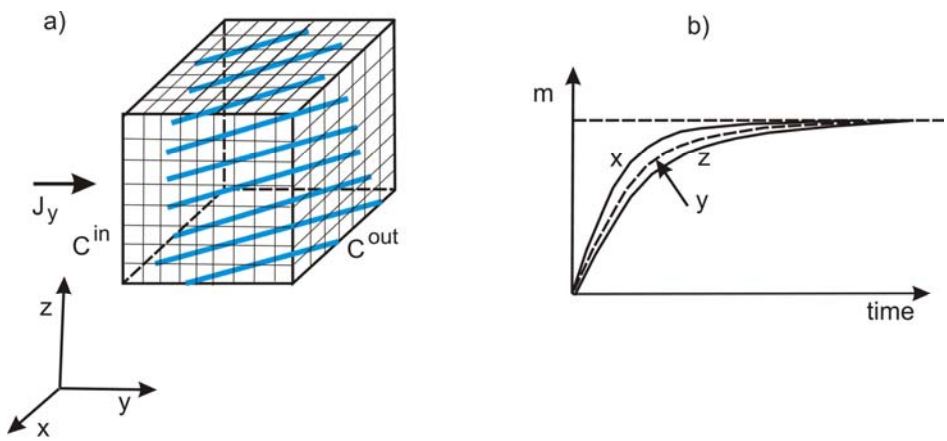

Fig. 4. Calculation of diffusion through reference volume. a) Internal structure of the reference volume (RV) assuming diffusion in y-direction due to concentration difference between C^{in} and C^{out}, the inlet and outlet flux is the same (equal J_y); b) Mass release curves for diffusion in three coordinate directions x,y,z.

Next, we calculate diffusion through the reference volume using equivalent quantities of a porous homogenous medium within the RV. The porosity *n* is evaluated from the internal structure of the RV. For each diffusion direction *i* (i.e. x,y,z), the steps are as follows:

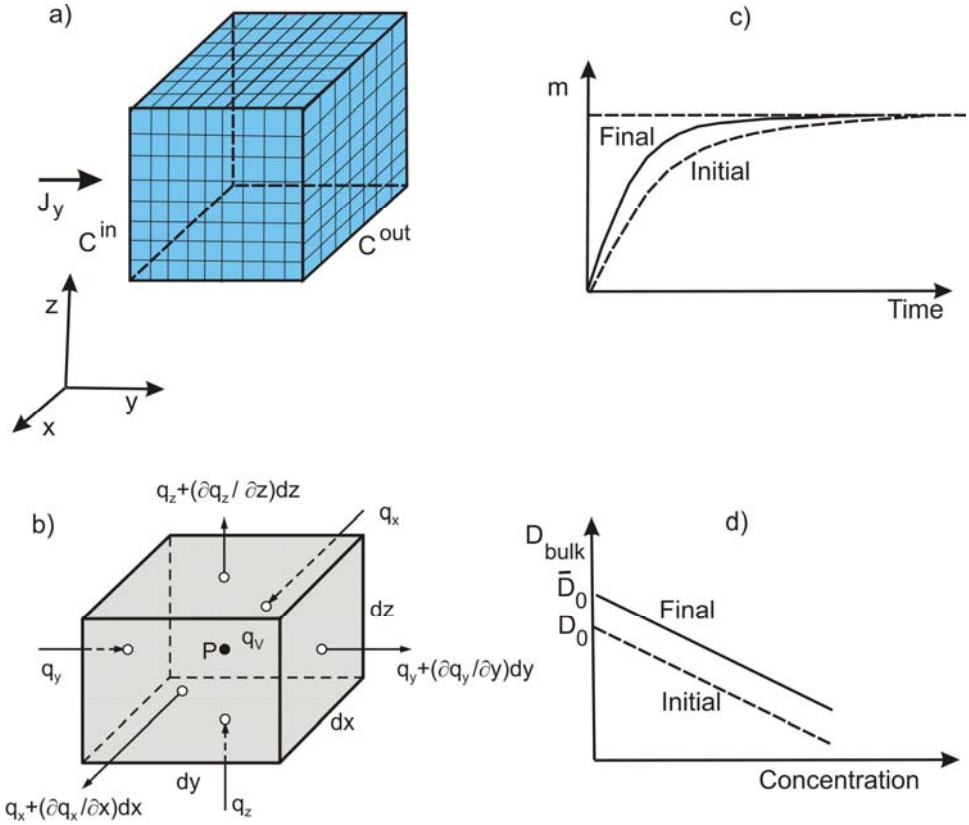

Fig. 5. Calculation of diffusion in equivalent homogenous porous medium. a) Reference volume;

b) Reference volume in deriving mass balance in differential form (analogy with RV for numerical calculation of equivalent material parameters), q_x, q_y, q_z are surface fluxes, and q_V is volumetric flux; c) Initial and final mass release curve, coinciding with the true mass release curve shown in Fig. 4b; d) Assumption about dependence of diffusion coefficient D_{bulk} on concentration – the slope of the line $D_{bulk}(c)$ is the same for the true and equivalent model.

1. Calculate mass release using initial diffusion using given $D_{bulk}(c)$.

2. Perform changes on the value D_0 until the mass release curve is close enough to the true curve, when the value is $(\bar{D}_0)_i$.

3. Using $(\bar{D}_0)_i$ calculate initial mass release curve taking into account equivalent values of the transformation matrix $\bar{\mathbf{T}}$ and equivalent distance from the solid surface $(\bar{h}_0)_i$.

4. Search for the distance $\bar{h}_i$ when difference between the calculated and true mass release curves is within a selected error tolerance.

In the above calculations of the equivalent transformation matrix and initial equivalent distance $\left(\overline{h}_0\right)_i$ a weighted procedure, which takes into account volumes belonging to FE nodes, is implemented (details not given here).

The presented concept of evaluation of parameters related to equivalent homogenous porous medium represents a numerical homogenization procedure. It can be extended to non-homogenous media, by varying equivalent parameters, or to stochastic characteristics. Application of introduced numerical homogenization method (NHM) is illustrated in the Results section.

2. Transport by fluid flow

We here consider two types of transport by fluid flow: 1) transport of rigid of deformable solids, and 2) transport by fluid with diffusion.

2.1 Transport of rigid and deformable bodies

In this case, we consider biological conditions where the fluid represents blood, rigid particles are taken to be nano-micro particles, while deformable particles represent biological cells (as red or white blood cells). This type of mass transport is of particular interest in blood flow within tumors, with blood vessels shown in Fig 6.

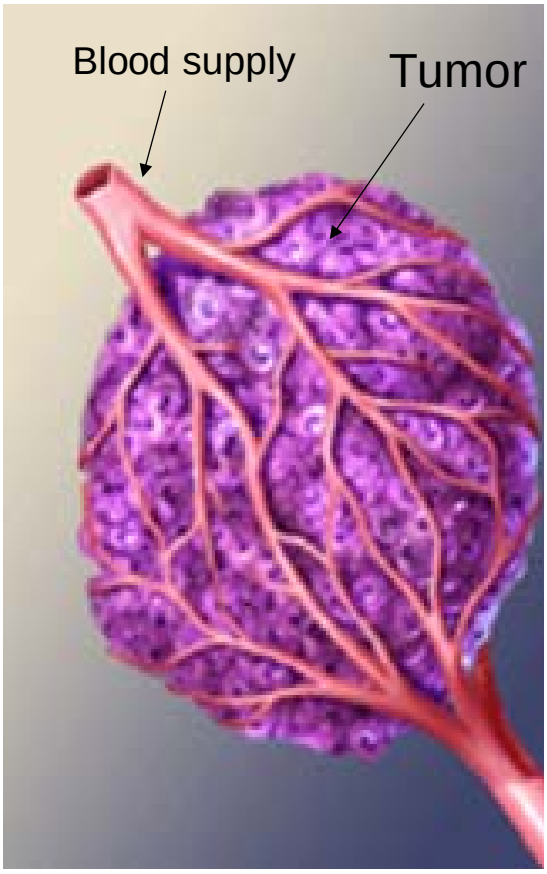

Fig. 6. Blood vessels supplying a tumor

Modeling of motion of bodies within a fluid has been the subject of intensive investigation in last decades. Generally, the models of solid-fluid interaction can be divided into two groups: loose coupling and strong coupling [Kojic et al. 2008a]. In the first group, solutions are obtained by solving separately for velocities and pressures of fluid using (with interpolation) velocities at the solid boundary; then, interaction forces acting from fluid are used to calculate dynamics of motion of solid. This procedure is repeated over time steps.

The strong coupling approach is designed to solve within the same system of equations for both fluid and solid domains. One of recent and popular methods is the so-called immersed boundary finite element method [Zhang et al. 2004], where the fluid equations are modified in the domain of solid and the solution is obtained by employing a stationary fluid FE mesh in the whole solid-fluid domain.

We have been employing a remeshing approach, as a strong coupling concept, and have developed software within the PAK package [Kojic et al. 1998, 2008] for modeling motion of solids within a fluid. Currently we have tested the methodology and software for 2D problems. The incremental equations for a solid finite element are:

$$\left(\frac{1}{\Delta t}\mathbf{M} + \Delta t\, {}^{n+1}\mathbf{K}^{(i-1)}\right)\Delta\mathbf{V}^{(i)} = {}^{n+1}\mathbf{F}^{ext(i-1)} - {}^{n+1}\mathbf{F}^{\mathrm{int}(i-1)} \tag{12}$$

where $\mathbf{M}$ and $\mathbf{K}$ are the element mass and stiffness matrices, respectively; $\Delta\mathbf{V}$ are increments of nodal velocities at time step n and iteration i; $\mathbf{F}^{ext}$ and $\mathbf{F}^{\text{int}}$ are external and internal nodal forces; indices n and n+1 indicate start and end of time step; and Δt is the time step size. Incremental equations for fluid element are

$$\begin{bmatrix} \frac{1}{\Delta t}\mathbf{M} + {}^{n+1}\tilde{\mathbf{K}}_{vv}^{(i-1)} & \mathbf{K}_{vp} \\ \mathbf{K}_{vp}^{T} & \mathbf{0} \end{bmatrix} \begin{Bmatrix} \Delta\mathbf{V}^{(i)} \\ \Delta\mathbf{P}^{(i)} \end{Bmatrix} =$$

$$\begin{Bmatrix} {}^{n+1}\mathbf{F}^{ext(i-1)} \\ 0 \end{Bmatrix} - \begin{bmatrix} \frac{1}{\Delta t}\mathbf{M} + {}^{n+1}\mathbf{K}_{vv}^{(i-1)} & \mathbf{K}_{vp} \\ \mathbf{K}_{vp}^{T} & 0 \end{bmatrix} \begin{Bmatrix} {}^{n+1}\mathbf{V}^{(i-1)} \\ {}^{n+1}\mathbf{P}^{(i-1)} \end{Bmatrix} + \begin{Bmatrix} \frac{1}{\Delta t}\mathbf{M}\,{}^{n}\mathbf{V} \\ 0 \end{Bmatrix} \tag{13}$$

with $$\left[{}^{n+1}\left(\tilde{\mathbf{K}}_{vv}^{(i-1)}\right)_{KJ}\right]_{ik} = \left[{}^{n+1}K_{KJ}^{(i-1)}\right]_{ii} + \left[{}^{n+1}J_{KJ}^{(i-1)}\right]_{ik}$$

$$\left[{}^{n+1}J_{KJ}^{(i-1)}\right]_{ik} = \rho\int_{V} N_K\,{}^{n+1}v_{i,k}^{(i-1)} N_J\,dV$$

where $\mathbf{P}$ is the nodal pressure vector and ρ is fluid density; matrices are defined elsewhere (Kojic et al. 2008a).

In the remeshing procedure we have that for a current time step the nodes at the solid-fluid interface are common and the FE matrices and nodal vectors from (12) and (13) are packed into the same system matrices and vector in a usual way. After the convergence is reached, the solid is displaced and remeshing of the fluid domain is performed, with common nodes at the interface, followed by mapping of the solutions from the previous to the new fluid mesh. Although these updates require additional time consuming calculations, we found that this approach is the most reliable and accurate with respect to other methods.

2.2 Transport by fluid with diffusion

In this case the overall transport of mass, consisting of small particles, as molecules in biology, represents a superposition of convective transport due to fluid flow and diffusion within the fluid. The mass distribution within the fluid is described by mass concentration. For dilute systems, transported mass does not affect the fluid flow, hence the above eqs. (13) are applicable. Besides these, additional equations for the concentration field can be derived in a differential form and then transformed into a FE format (see, e.g. Kojic et al. 2008a):

$$\mathbf{M}_j\dot{\mathbf{C}}_j + \mathbf{K}_j\mathbf{C}_j + \mathbf{K}_{Cjv}\mathbf{V} = \mathbf{Q}_j^S + \mathbf{Q}_j^V \qquad \text{no sum on } j \tag{14}$$

for a mass constituent 'j'. Here $\mathbf{C}$ and $\mathbf{V}$ are vectors of nodal concentrations and velocities, respectively; first two terms correspond to diffusion, while the third term represents the convective contribution; vectors on the right hand side are surface and volumetric mass fluxes. Detailed specification of matrices and vectors is given elsewhere (Kojic et al. 2008a).

3. Examples

With few examples we illustrate applications of the above theoretical considerations.

3.1 Diffusion

Example 1. Diffusion within medium with parallel fibers. This example is typical to show the extreme differences in equivalent quantities corresponding to flux parallel to fibers and orthogonal to fibers. The reference volume with fibers is shown in Fig. 7.a. Data are given in the figure caption, including the calculated initial equivalent distance from surface $\bar{h}$.

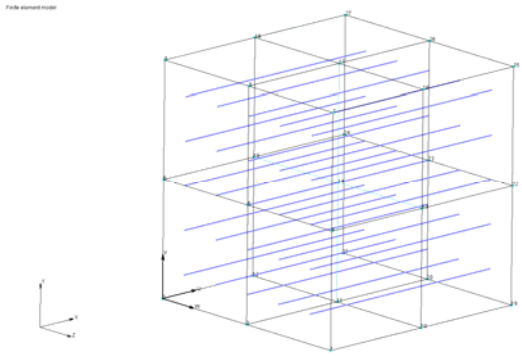

a)

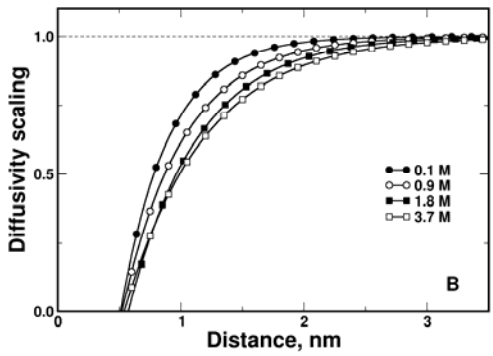

b)

Fig. 7. a) Reference volume with 25 fibers parallel to x-axis. **Data:** dimensions: $L_n = W_n = D_n = 0.04\mu m$; diffusion coefficient line: D_0^1 = 5.9616e+7 for c=0, D_0^2 = 1.9008e+7 $\mu m^2 / s$ for c=2.75M; porosity: 0.693204; initial equivalent distance from surface $\bar{h}$ = 0.001073 μm ; b) Scaling functions for glucose in silica nanochannels (according to Ziemys et al. 2011).

Figure 8 shows mass flux distribution at time t=4.e-4 *s* in x- and y-direction in case of diffusion in x-direction. Note that maximum flux in y (or z) direction is around two orders of magnitude smaller than in x-direction. The initial and the final (after the solution for $\bar{D}_0$ is obtained) mass release curves are practically the same in case of neglected surface effects (curve x-D(c) in

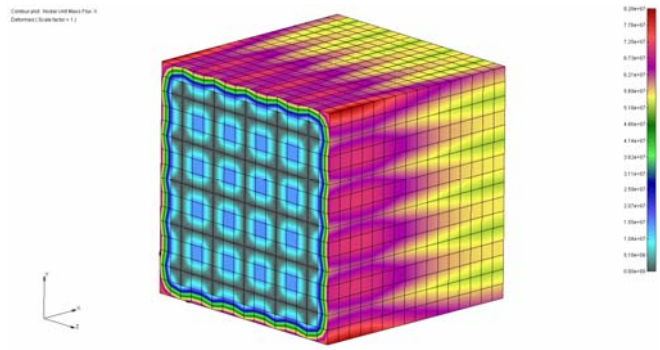

a)

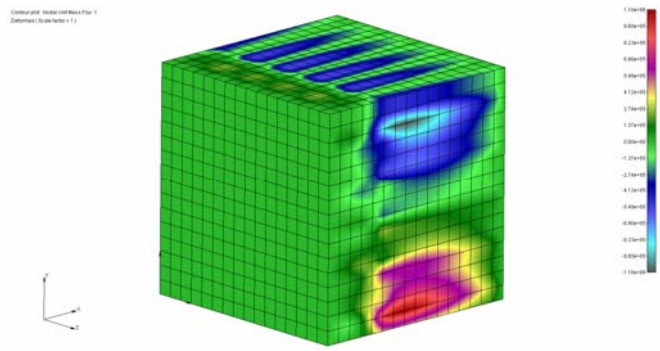

b)

Fig. 8. Mass flux distribution within reference volume of Fig. 7a at time t=4.e-4 *s* in case of diffusion in x-direction. a) Flux in x-direction, maximum value shown in red color is 8.28e+7 $fg / \mu m^2$; b) Flux in y-direction, maximum value, given in red color is 1.1e+6 $fg / \mu m^2$.

Fig.11); this can be seen from the D(c) lines in Fig. 9a. The initial and final mass release curves in case of surface effects are shown in Fig. 9b. The final equivalent distance from surface is 0.001228 μm (larger than the initially determined, equal to 0.001073).

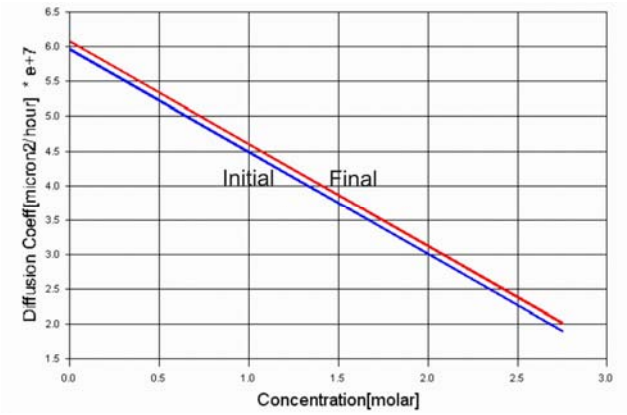

a)

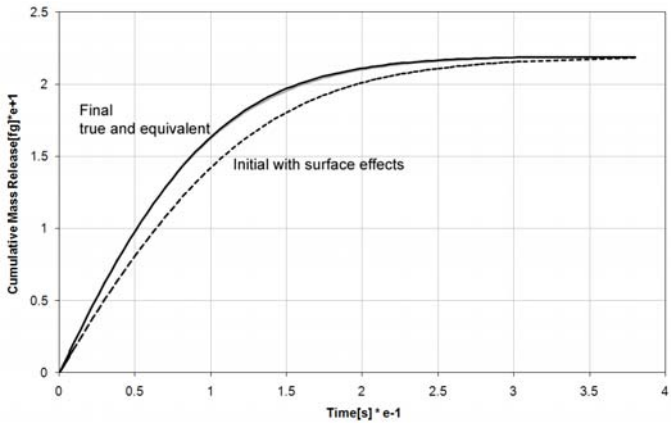

b)

Fig. 9. Diffusion in x-direction. a) Initial and final D(c) dependence in case of neglected surface effects; b) Initial and final mass release curves with surface effects included.

Next, we calculate diffusion for this model when diffusion occurs in y-direction, i.e. orthogonal to fibers. Fluxes in y- and z-direction at time t=4.e-4 s are shown in Fig. 10. Flux in x-

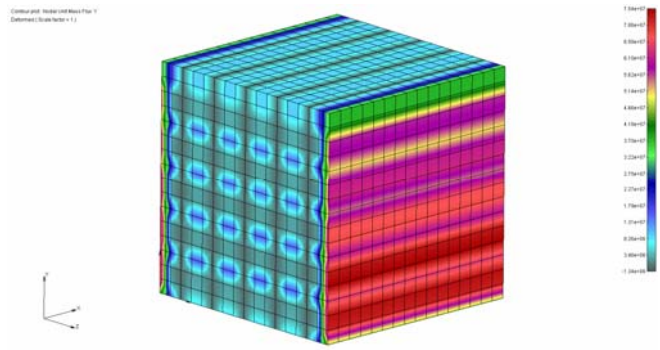

a)

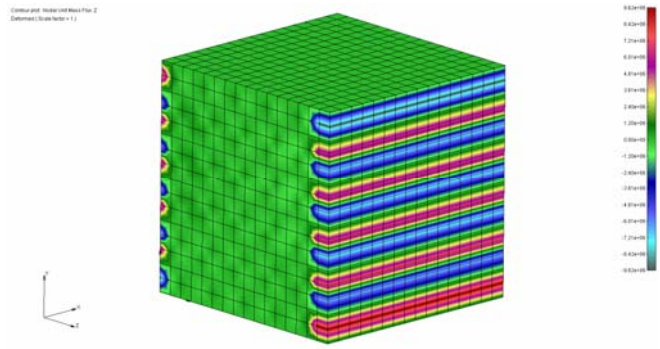

b)

Fig. 10. Diffusion in y-direction, fluxes at time t=4.e-4 s a) Flux y-direction, maximum value is 7.54e+7 $fg / \mu m^2$; b) Flux in z-direction, maximum value is 9.26e+6 $fg / \mu m^2$.

direction is approximately equal to zero. Now, the initial and final bulk diffusion coefficients are significantly different, as can be seen from Fig. 11.a. The mass release curves for initial and final

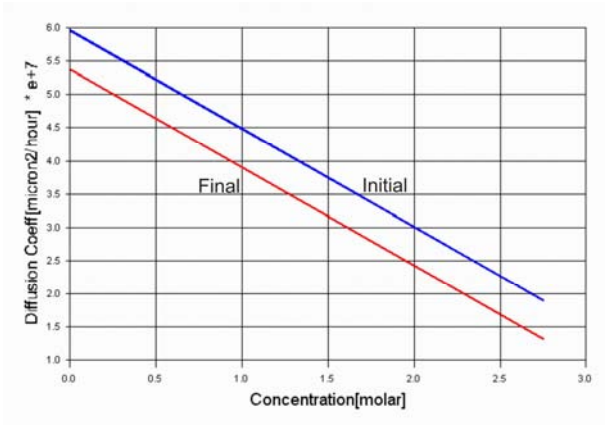

a)

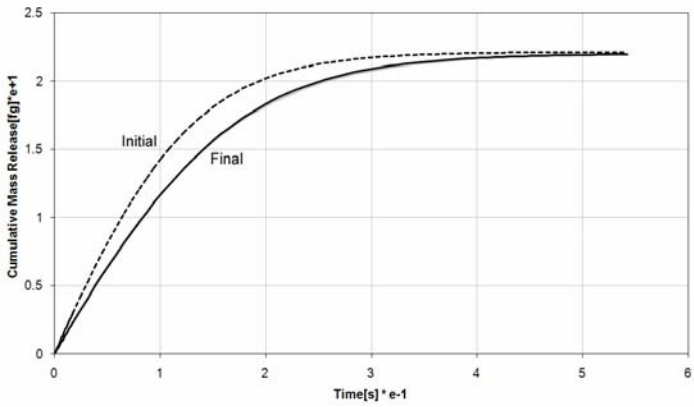

b)

Fig. 11. Diffusion in y-direction. a) Initial and final D(c) dependence in case of neglected surface effects; b) Initial and final mass release curves with surface effects included.

values of $\overline{h}$ are shown in Fig. 11b. The final equivalent distance from surface is 0.000982 μm (smaller than the initially determined, equal to 0.001073, and smaller then for diffusion in x-direction equal to 0.001228). Hence the surface effects are more pronounced when diffusion is in the y-direction.

A summary of results for this example is given in Fig. 11. It can be seen that there is no significant difference in mass release between diffusion along fibers (x-direction) and diffusion normal to the fibers, when surface effects are neglected. However, this difference is notable if the surface effects are taken into consideration.

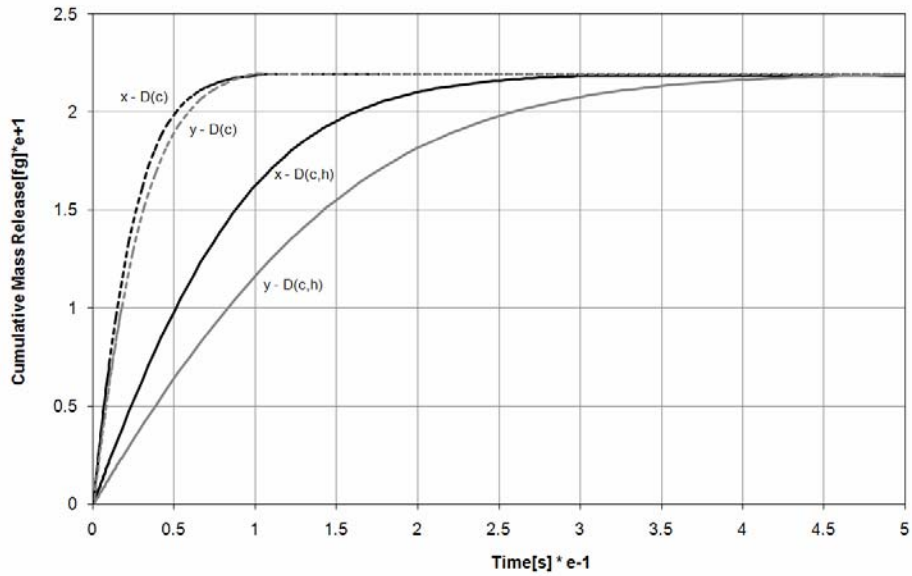

Fig. 12. Mass release curves for diffusion within medium with fibers parallel to x-axis. Notation in the figure: x-D(c), y-D(c) diffusion in x- and y-direction in case when surface effects are neglected; x-D(c,h), y-D(c,h) diffusion in x- and y-direction with surface effects.

Example 2. Diffusion within medium with differently oriented sets of fibers and spherical solids. Composition of this complex medium is shown in Fig. 13. It consists of several sets of fibers and symmetrically displaced spherical solids.

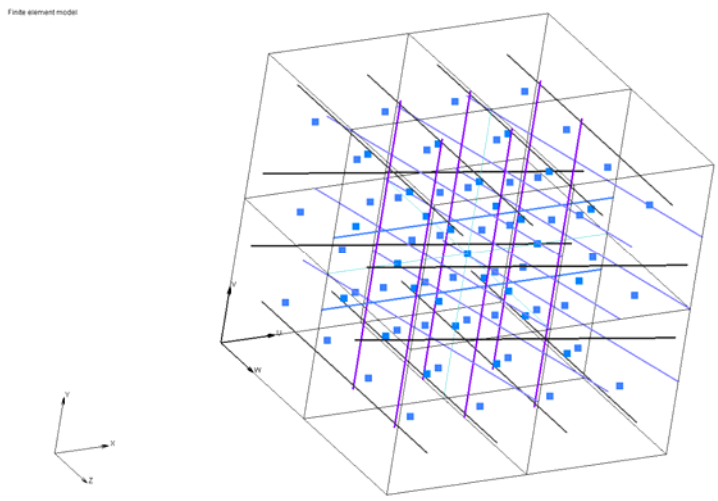

Fig. 13. Complex composite medium. **Data:** dimensions: $L_n = W_n = D_n = 0.04\mu m$; diffusion coefficient line: $D_0^1 = 1.656e{+}4$ for c=0, $D_0^2 = 5.280e{+}3\ \mu m^2 / s$ for c=2.75M; porosity: 0.853547; initial equivalent distance from surface $\bar{h} = 0.005447\ \mu m$.

In Figure 14 are given concentration field and field of flux in x-direction in case of diffusion in x-direction. A significant non-uniformity can be seen for both fields. Similar character of non-uniformity is found for diffusion in other two coordinate directions (not shown here).

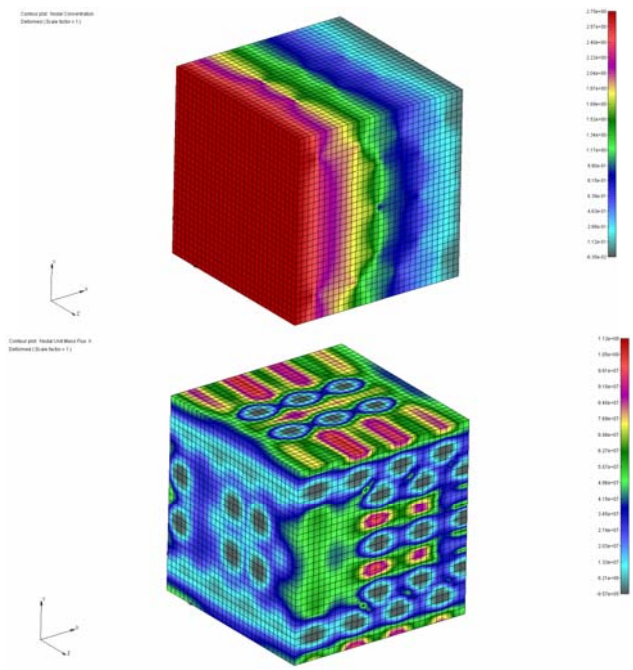

Fig. 14. Complex composite model. Fields of concentration (left) and x-fluxes (right) at time t=1E-3s, diffusion in x-direction.

Mass release curves for x,y,z directions are shown in Figure 15, with initial curves corresponding to the weighted value of distance from surface $\bar{h}$ = 0.005447 μm. It can be seen that

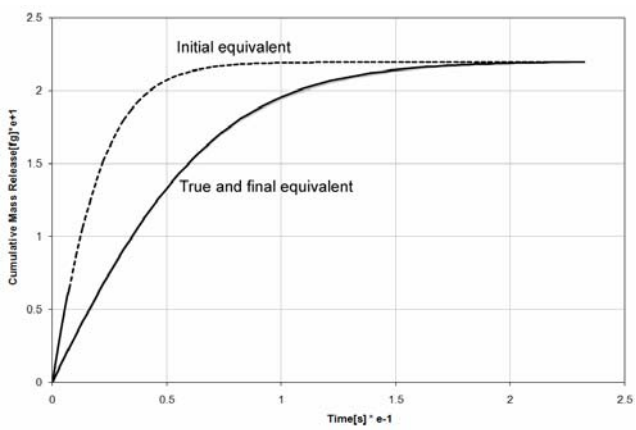

a) Diffusion in x-direction

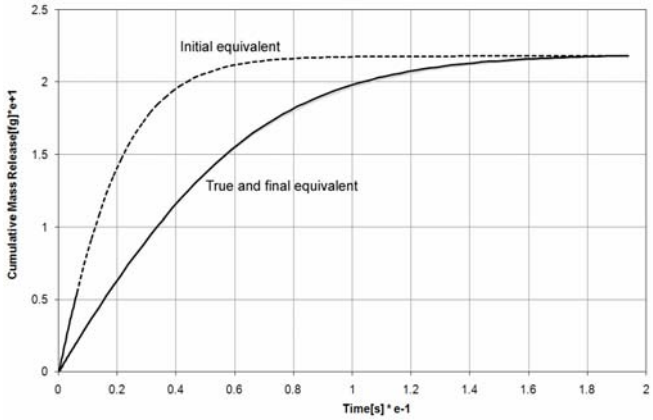

b) Diffusion in y direction

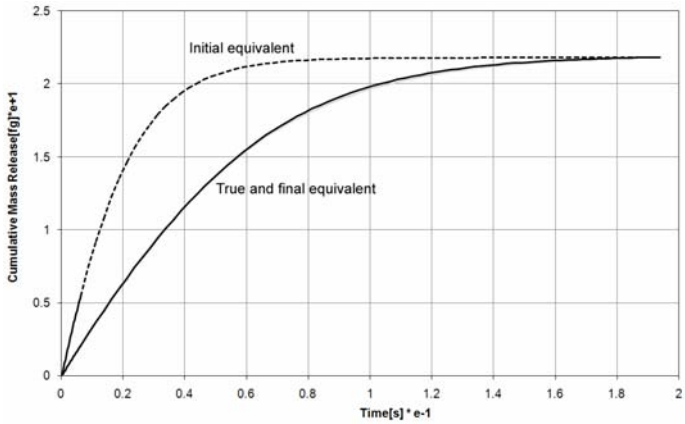

c) Diffusion in z-direction

Fig. 15. Mass release curves for the complex model assuming diffusion in three orthogonal directions.

there are no significant differences between the mass release curves. A summary of equivalent model parameters is given in Table 1. Since there is no significant difference in equivalent model parameters, the model has characteristics close to isotropic.

Table 1. Parameters for equivalent model

Diffusion direction	Equivalent distance from surface $\overline{h}$ (inital 0.005447) [μm]	Diff coefficient for c=0, initial 1.656e+4 [$\mu m^2 / s$]	Diff coefficient for c=2.75M initial 5.280e+3
x	0.001433	1.6353e+4	5.073e+3
y	0.001474	1.64560e+4	5.1765e+3
z	0.001493	1.64560e+4	5.1765e+3

3.2 Transport by fluid flow

Here, we consider motion of red blood cells within capillary narrowing, and transport and accumulation of proteins within a blood vessel segment.

Example 3. Motion of red blood cells and nanoparticles within a capillary narrowing. A capillary of diameter 20 μm has narrowing to diameter of 5 μm, as shown in Fig. 16. It is assumed that two red blood cells are initially at the same vertical position near the entrance, behind which are displaced 5 nanoparticles symmetrically positioned with respect to the axial axis. We use a 2D model

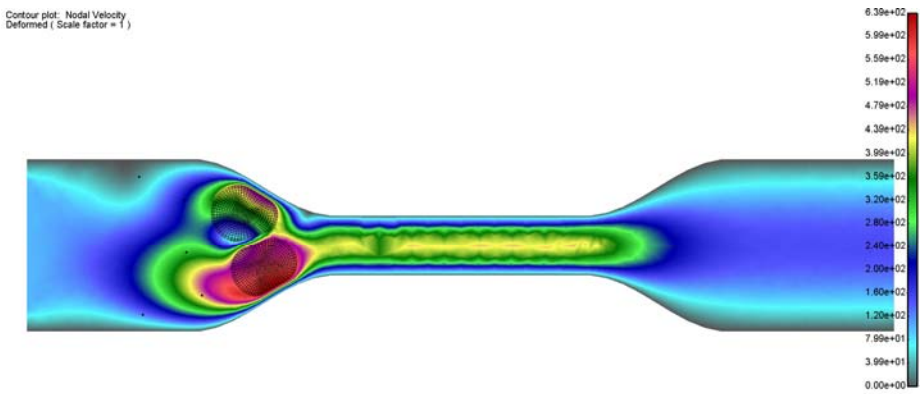

a) Entire domain

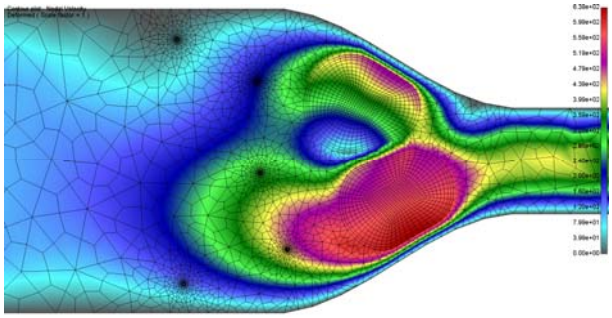

b) Position of circular particles

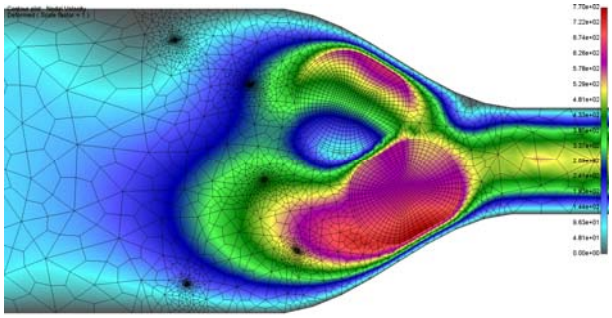

c) Position of elliptical particles

Fig. 16. Capillary with narrowing. Velocity distribution at the moment when RBC enter the narrowing. a) Entire domain; b) Domain at the narrowing entrance – position of circular particles; c) Domain at the narrowing entrance – position of elliptical particles.

for this problem. Two cases are considered: a) particles are circular, with diameter of 200*nm*, or b) elliptical with the same area as circular and with ellipse axes ratio 2:1. The RBCs are considered as homogenous elastic bodies with Young modulus $E = 200\,Pa$, density $\rho_s = 1.01 \cdot 10^3\, kg/m^3$, Poison ratio $\nu = 0.499$, while nanoparticles and vessel walls are taken to be rigid (very high elastic modulus). The fluid is assumed to be homogeneous and Newtonian, with density $\rho_f = 1.0 \cdot 10^3\, kg/m^3$ and dynamic viscosity $\mu = 3.675 \cdot 10^{-3}\, Pa\,s$.

Particle trajectories until the RBCs reach the outlet of the capillary are shown in Fig. 17.

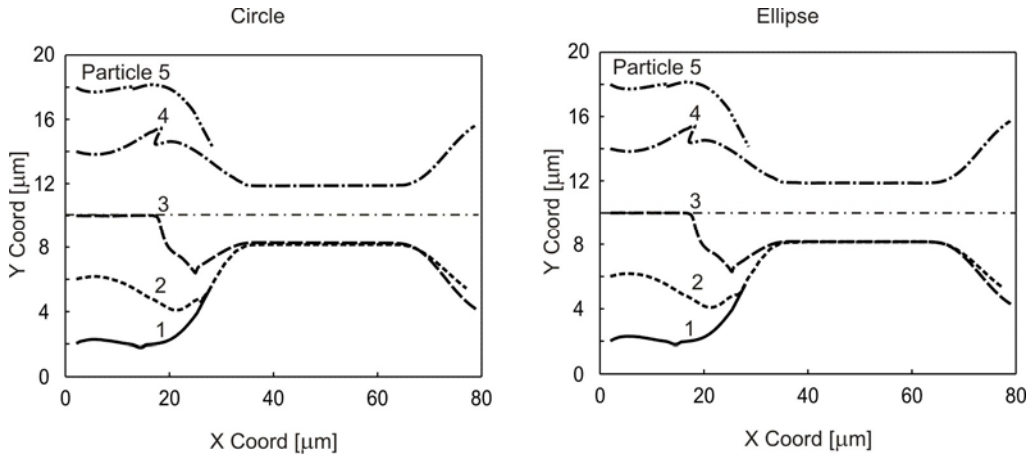

Fig. 17. Particle trajectories for circular (left) and elliptical (right).

It can be seen that the trajectories are practically the same for both types of particles. Figure 18 shows evolution of rotation during motion of particles. The positive sign of rotation is shown in the figure, and indicated for each particle. It is interesting to note that rotation is significantly slower for elliptical nanoparticles with respect to circular ones, while the trajectories are the same. Also, particle

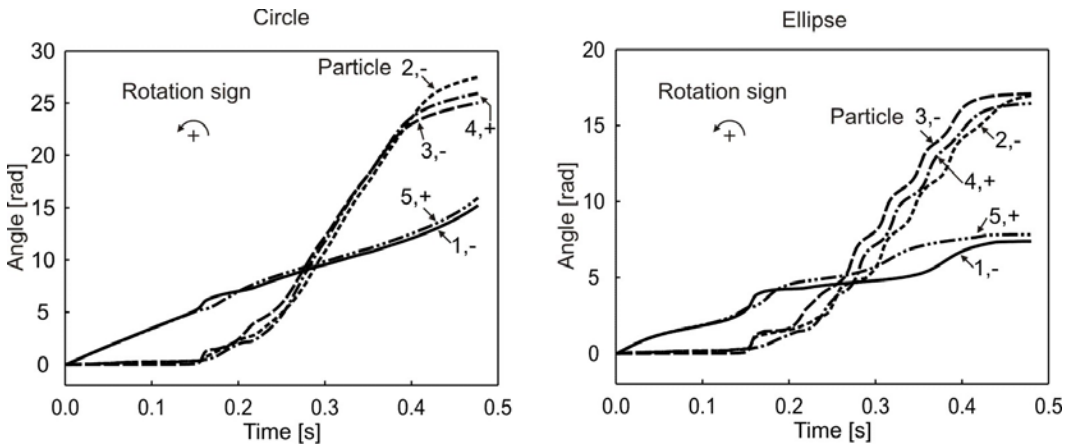

Fig. 18. Evolution of rotation of nanoparticles during motion within the blood

which initially is at the axis of symmetry experiences large rotation. Finally, particles 1 and 5 have larger rotations in the initial period with respect to 2, 3, 4 (which are further from the wall), and then the particles 2, 3, 4 experience large rotations while moving through the narrowing. This is due to the fact that rotation is produced by shear flow which is more pronounced in the wall vicinity.

Example 4. Transport and accumulation of proteins in isolated blood vessel. The following example calculates distribution of accumulated low density lipoprotein (LDL) molecule in different segments of the isolated blood vessel. Experiments of LDL transport were performed on the isolated rabbit common carotid artery. The blood vessel was stretched to its approximate in vivo length. The outer diameter of the blood vessel was measured using digital

camera and originally developed software. The blood vessel wall thickness was measured at the end of each experiment, using light microscope and microscopically graduated plate. Computer model of the artery is considered as a simple straight tube. The diameter of artery was D=0.0029m, the mean velocity U_0=0.24m/s, dynamics viscosity μ=0.0035Pa s, density ρ=1050 kg/m^3. The transmural pressure under normal physiological condition was taken as 70 mmHg.

Matching of histological data and computational simulation is presented in Fig. 19. The process of matching histological images was done by 2D deformation of each histological cross-section in order to keep the internal lumen approximately cylindrical shape. The maximum LDL was found at distal part of the carotid artery segment at 3.5 mm from entry segment. A full three-dimensional finite element analysis was performed using our in-house finite element code in order wall shear stress and function of permeability for the wall. Oxidized LDL, macrophages and cytokines distribution is presented in Fig. 20. Experimental LDL transport of 15.7% was fitted with specific nonlinear least square analysis [Chavent, 2010] in order to obtain numerical parameters.

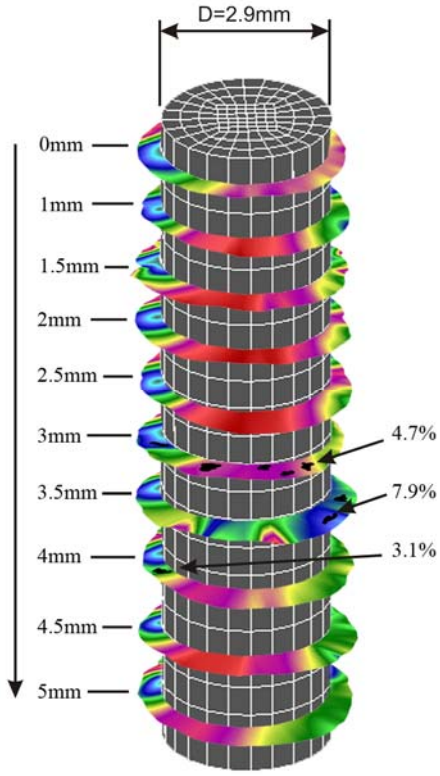

Fig. 19. Labeled LDL located in histology cross-section on each 0.5 mm for straight segment. Histology segments were obtained as deformable elastic rings opened from the current squeezed position to circle original tube. Black holes in these cross-sections show location of the labeled LDL. Percentages show labeled LDL area inside media and intima wall thickness.

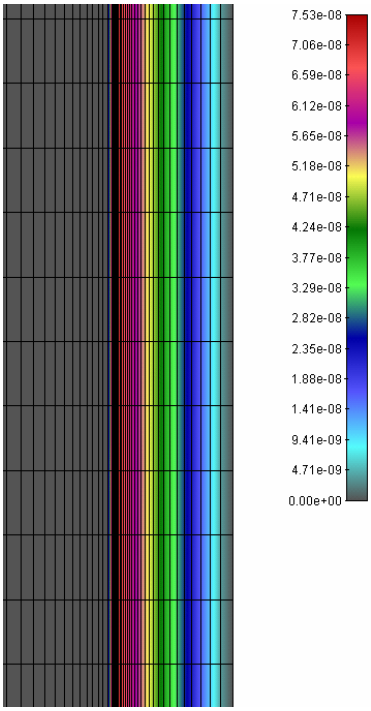
7.53e-08
7.06e-08
6.59e-08
6.12e-08
5.65e-08
5.18e-08
4.71e-08
4.24e-08
3.77e-08
3.29e-08
2.82e-08
2.35e-08
1.88e-08
1.41e-08
9.41e-09
4.71e-09
0.00e+00

a)

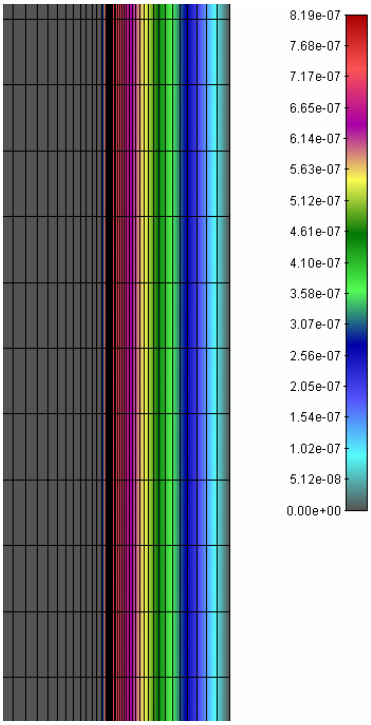
8.19e-07
7.68e-07
7.17e-07
6.65e-07
6.14e-07
5.63e-07
5.12e-07
4.61e-07
4.10e-07
3.58e-07
3.07e-07
2.56e-07
2.05e-07
1.54e-07
1.02e-07
5.12e-08
0.00e+00

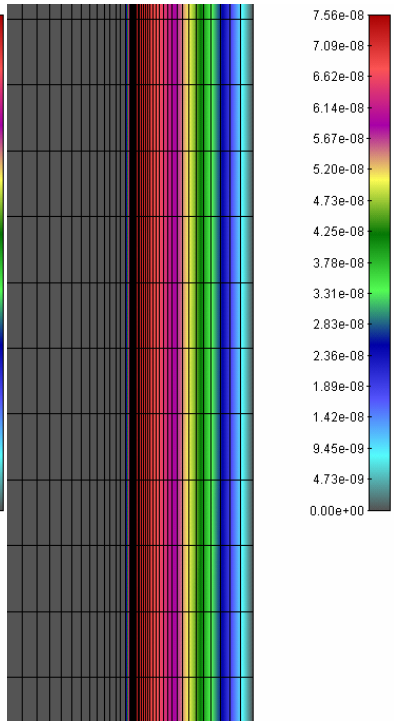
7.56e-08
7.09e-08
6.62e-08
6.14e-08
5.67e-08
5.20e-08
4.73e-08
4.25e-08
3.78e-08
3.31e-08
2.83e-08
2.36e-08
1.89e-08
1.42e-08
9.45e-09
4.73e-09
0.00e+00

b) c)

d)

Fig. 20 a) Oxidized LDL distribution 0.37%; b) Macrophages distribution 4.2% from media; c) Cytokines distribution 0.39%; d) three-dimensional representation of the model

3. Conclusions

Based on the hierarchical model for diffusion [Ziemys et al. 2011], which couples MD and macroscale FE methods, we have presented an extension of the model to include adsorption at the surfaces bounding the nano-scale diffusion domain.

Also, a concept of generalization of the model to diffusion through porous media is outlined. This generalized model can lead to development of multiscale models applicable to diffusion in biological environment, as it is in intracellular space, or polymers. Development of these models will certainly require solution of many challenging tasks.

We have further presented methodologies for modeling of motion of rigid and deformable solids in fluids, based on a remeshing procedure. This solution concept of managing solid-fluid interaction is applied to modeling of RBCs and nanoparticles in a capillary with narrowing. Being reliable and accurate, this methodology provides a tool for investigation of various processes in biomedicine.

Finally, a standard FE approach in modeling transport of small particles (molecules) by calculating concentration fields coupled with convection by fluids is outlined and implemented to one of current investigation tasks within the ARTreat EU grant. Other examples and details are given elsewhere, e.g. [Filipovic et al., 2011].

Acknowledgements

This project has been supported with federal funds from NASA under the contracts NNJ06HE06A and NNX08AW91G, Department of Defense under the contract DODW81XWH-09-1-0212, as well as funds from State of Texas Emerging Technology Fund, Nano Medical Systems (NMS), Alliance of NanoHealth (ANH), and University of Texas at

Houston. The authors acknowledge the Texas Advanced Computing Center (TACC) at The University of Texas at Austin for providing HPC resources that have contributed to the research results reported within this paper.

The authors acknowledge support from Ministry of Education and Science of Serbia, grants OI 174028 and III 41007, City of Kragujevac, and from FP7-ICT-2007 project (grant agreement 224297, ARTreat).

Извод

Транспорт у биолошким системима

M. Kojic[1,2], A. Ziemys[2], M. Milosevic[1], V. Isailovic[1], N. Kojic[4,5], M. Rosic[3], N. Filipovic[3], M. Ferrari[2]

[1]Metropolitan University, Belgrade – R & D Center for Bioengineering, 34000 Kragujevac, Serbia
[2]The Methodist Hospital Research Institute, Houston, TX 77030
[3]University of Kragujevac
[4]Tufts University, Medford, MA 02155, 5 – Metropolitan University, Belgrade

Резиме

Транспорт материје у биолошким системима представља витални и најзначајнији процес. Транспорт се догађа на различитим скалама, у распону од атомске до макроскале. Он је врло сложен пошто обухвата биохемијске и механичке изворе. Моделирање је још увек изазов услед ове сложености. У овом раду се осврћемо на следеће специфичне теме: дифузију у комплексним срединама, транспорт солидних тела флуидом, и транспорт дистрибуиране материје флуидом. Ово су теме на којима се раде истраживања у Истраживачком институту Методист болнице у Хјустону; и у Мтерополитан универзитету Београд – Истраживачко развојном центру за биоинжењеринг у Крагујевцу. Методологија за дифузију се заснива на хијерархијском прилазу моделирања уведеног у [Зиемус и други 2011] који узима у обзир међуповршинске ефекте између солидне фазе и молекула који се транспортују.

Овде се предлаже генерализација хијерархијског прилаза на дифузију у композитним срединама. Употребљавамо поступак ажурирања мреже за моделирање кретања деформабилних тела (биолошке ћелије, као што су црвена крвна зрнца) или крутих тела (нано- или микро-делићи) у флуиду као што је крвна течност. Користимо једначине транспорта, које повезују кретање флуида и дифузију, за транспорт дистрибуиране материје као што су биолошки протеини у крви.

Кључне речи: дифузија, молекуларни транспорт, молекуларна динамика, метод коначних елемената, транспорт биолошких ћелија, метод са ажурирањем мреже, транспорт дистрибуиране материје

References

Ziemys A, Kojic M, Milosevic M, Kojic N, Hussain F, Ferrari M, Grattoni A (2011). Hierarchical modeling of diffusive transport through nanochannels by coupling molecular dynamics with finite element method, Journal of Computational Physics, 230, 5722–5731.

Kojic M, Milosevic M, Kojic N, Ferrari M, Ziemys A. (2011) On diffusion in nanospace, J. Serbian Soc. Comput. Mechanics, 84-95.

English, A. and M. Dole, Diffusion of sucrose in supersaturated solutions. Journal of the American Chemical Society, 1950. 72(7): p. 3261-3267.

Alpert, S. and G. Banks, The concentration dependence of the hemoglobin mutual diffusion coefficient. Biophysical Chemistry, 1976. 4(3): p. 287-296.

Ziemys, A., et al., Confinement Effects on Monosaccharide Transport in Nanochannels. The Journal of Physical Chemistry B, 2010: p. 132-137.

Aggarwal, N., J. Sood, and K. Tankeshwar, Anisotropic diffusion of a fluid confined to different geometries at the nanoscale. Nanotechnology, 2007. 18(33): p. 5.

Rudd, R. and J. Broughton, Coarse-grained molecular dynamics and the atomic limit of finite elements. Physical Review B, 1998. 58(10): p. 5893-5896.

Hou, T. and X. Wu, A Multiscale Finite Element Method for Elliptic Problems in Composite Materials and Porous Media* 1. Journal of Computational Physics, 1997. 134(1): p. 169-189.

Broughton, J., et al., Concurrent coupling of length scales: Methodology and application. Physical Review B, 1999. 60(4): p. 2391-2403.

Wagner GJ, Liu WK (2003). Coupling of atomistic and continuum simulations using a bridging scale decomposition, J. Comput. Phys., 190, 249-274

Kojic M, Filipovic N, Tsuda A (2006a). A multiscale method for bridging dissipative particle dynamics and Navier-Stokes finite element equations for incompressible fluid and its application in biomechanics. Proc. First South-East European Conference on Comp. Mechanics (Eds. M. Kojic and M. Papadrakakis), Kragujevac, Serbia.

Kojic M, Filipovic N, Stojanovic B, Kojic N (2008a). Computer Modeling in Bioengineering: Theoretical background, examples and software. 200, 8: John Wiley & Sons.

Kojic M, Filipovic N, Tsuda A (2008b). A mesoscopic bridging scale method for fluids and coupling dissipative particle dynamics with continuum finite element method, Comp. Meth. Appl. Mech. Engrg., 197, 821-833.

Rapaport DC (2004). The Art of Molecular Dynamics Simulation, Cambridge University Press

MacKerell Jr, A., et al., All-Atom Empirical Potential for Molecular Modeling and Dynamics Studies of Proteins†. Journal of Physical Chemistry B, 1998. 102(18): p. 3586-3616.

Ziemys, A., M. Ferrari, and C.N. Cavasotto, Molecular Modeling of Glucose Diffusivity in Silica Nanochannels. Journal of Nanoscience and Nanotechnology, 2009. 9: p. 6349-6359.

Phillips, J.C., et al., Scalable molecular dynamics with NAMD. J Comput Chem, 2005. 26(16): p. 1781-1802.

Jorgensen, W.L., et al., Comparison of simple potential functions for simulating liquid water. Journal of Chemical Physics, 1983. 79(2): p. 926-935.

Cruz-Chu, E.R., A. Aksimentiev, and K. Schulten, Water-silica force field for simulating nanodevices. J Phys Chem B, 2006. 110(43): p. 21497--21508.

Gladden, J.K. and M. Dole, Diffusion in supersaturated solution-II: glucose solutions. J. Am. Chem. Soc., 1953. 75: p. 3900-3904.

Bathe, K., Finite element procedures. 1996, Englewood Cliffs, New Jersey: Prentice-Hall.

Hughes, T., The finite element method: linear static and dynamic finite element analysis. 2000, New York: Dover Publications.

Kojic, N., A. Kojic, and M. Kojic, Numerical determination of the solvent diffusion coefficient in a concentrated polymer solution. Communications in Numerical Methods in Engineering, 2006b. 22(9): p. 1003-1013

Kojic M., Filipovic, N., Stojanovic, B. and Kojic N. (2008), Computer Modeling in Bioengineering,
Theoretical Background, Examples and Software, J Wiley and Sons, Chichester.

Fine, D., et al., A robust nanofluidic membrane with tunable zero-order release for implantable dose specific drug delivery. Lab on a Chip, 2010.

Zhang, L., Gerstenberger, A., Wang, X. and Liu, W. K. (2004), "Immersed finite element method", Comput. Methods Appl. Mech. Engrg., 193, pp. 2051-2067.

Kojic M, Slavkovic R, Grujovic N, Zivkovic M, Filipovic N. (1998, 2009) PAK – FE program for linear and nonlinear analysis for solids, fluids, mass and heat transfer, biomechanics and coupled problems; Mech. Eng. Faculty, University of Kragujevac; R & Center for Bioengineering, Kragujevac, Serbia.

View publication stats